SUPPORTING INFORMATION

TOWARDS THE MODELING OF QUANTUM-DOT SENSITIZED SOLAR CELLS: FROM STRUCTURAL AND VIBRATIONAL FEATURES TO ELECTRON INJECTION THROUGH LATTICE-MISMATCHED INTERFACES

Alexandra Szemjonov[1], Thierry Pauporté[1], Sandrine Ithurria[2], Silvia Pedetti[2], Nicolas Lequeux[2], Benoit Dubertret[2], Ilaria Ciofini*[1], Frédéric Labat*[1]

[1] *Chimie ParisTech, PSL Research University, CNRS, Institut de Recherche de Chimie Paris (IRCP), 11 Rue Pierre et Marie Curie, F-75005 Paris, France*
[2] *Laboratoire de Physique et d'Etude des Matériaux, UMR 8213 du CNRS, ESPCI, 10 rue Vauquelin, 75231 Paris, France*

* ilaria.ciofini@chimie-paristech.fr
* frederic.labat@chimie-paristech.fr

Calculation of TO and LO Raman frequencies with the CRYSTAL code:

The eigenvalues obtained by the diagonalization of the mass-weighted *W* matrix correspond to the TO frequencies. *W* is then corrected with a term W^{NA} that depends on the cell volume, the dynamic dielectric tensor and the Born effective charges, as described in ref.1, and the LO frequencies correspond to the eigenvalues obtained by the diagonalization of the $W+W^{NA}$ matrix. The correspondance between the LO and TO modes is established based on the maximum overlap between LO and TO modes. However, the TO and LO vectors originate from independent diagonalizations, and do not belong to the same orthonormal set. Therefore, a TO mode from one orthonormal set of vectors and the corresponding LO mode from another one might not have a mutual maximum overlap with each other, preventing us from making a one-to-one correspondence between the two. Due to the high symmetry of bulk compounds, it was possible to compute the LO/TO splitting in their Raman spectra with the chosen computational protocol. This was not the case for the low-symmetry slabs, therefore we deduced their LO frequencies by adding the corresponding bulk LO/TO splitting values to their TO frequencies.

1 C. M. Zicovich-Wilson, F. J. Torres, F. Pascale, L. Valenzano, R. Orlando and R. Dovesi, *J. Comput. Chem.*, 2008, **29**, 2268–2278.

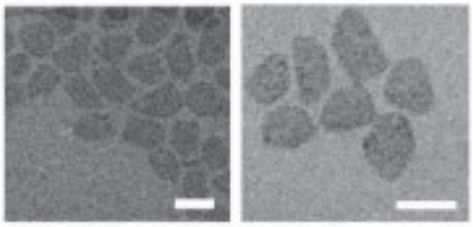

a) *b)*

Figure S1. TEM views of a) 9 and b) 13 layers thick CdSe nanoplatelets

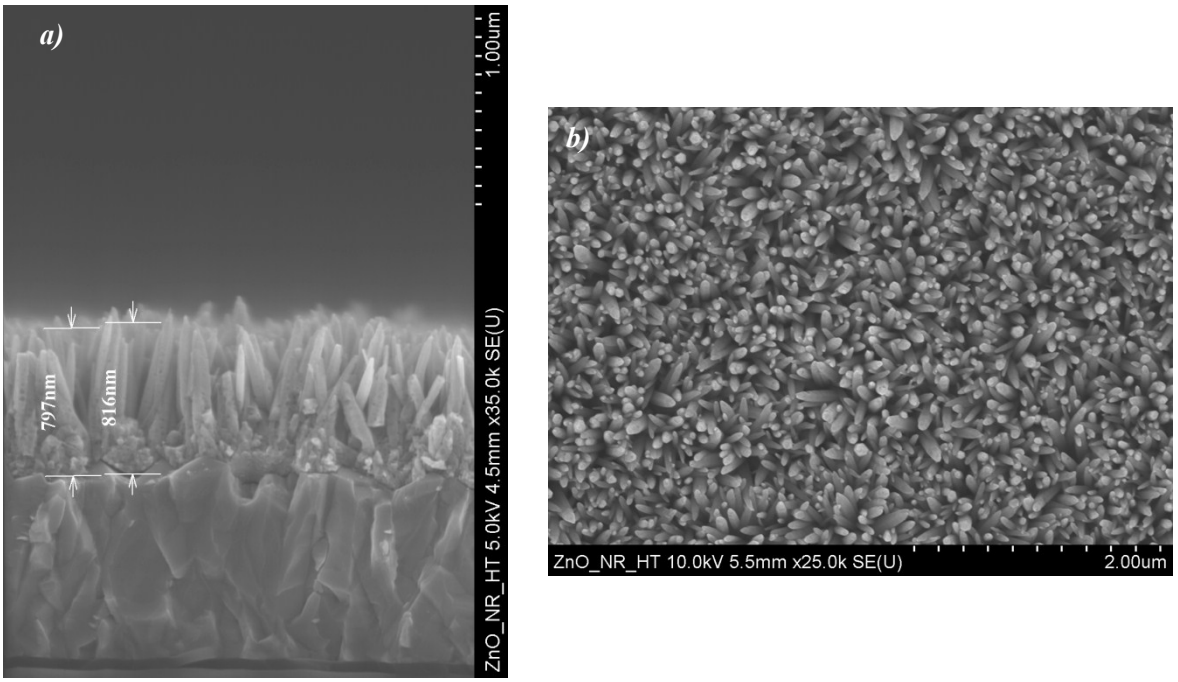

Figure S2. a) Cross-sectional and b) top SEM views of hydrothermally grown ZnO nanorod arrays

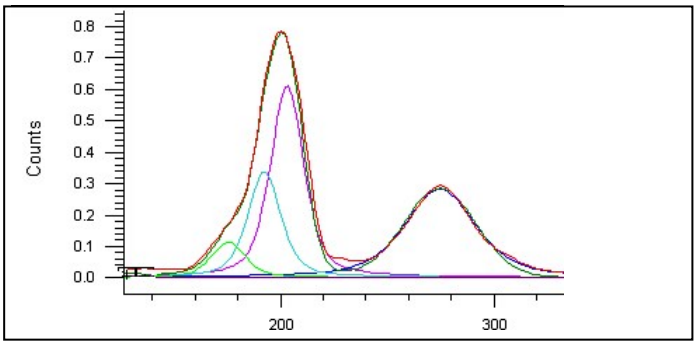

Curve name	Centre (nm)	Width (nm)	Height (counts)	% Gaussian
CdS interface	274.6	39.66	0.2839	100
CdSe bulk LO	202.9	18.30	0.6198	100
CdSe SO	192.3	18.30	0.3399	50
CdSe TO	175.4	18.30	0.1147	50

Figure S3. Decomposition of the CdSe- and CdS-related peaks in the experimental Raman spectra of 9 layers thick CdSe.SH NPLs.

a)

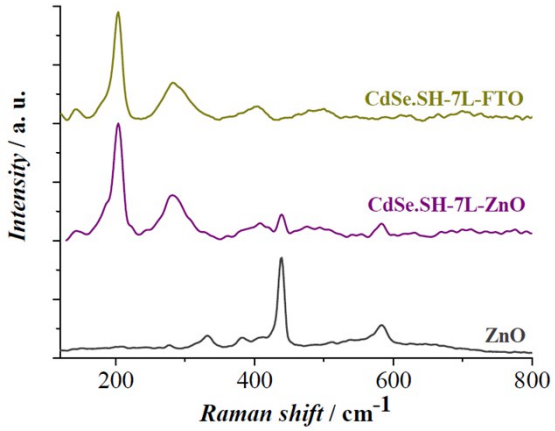

b)

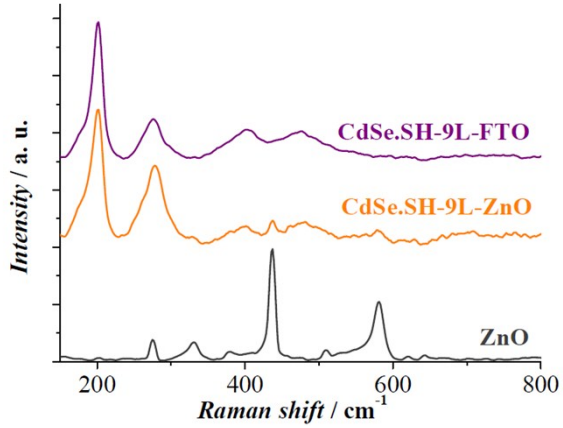

c)

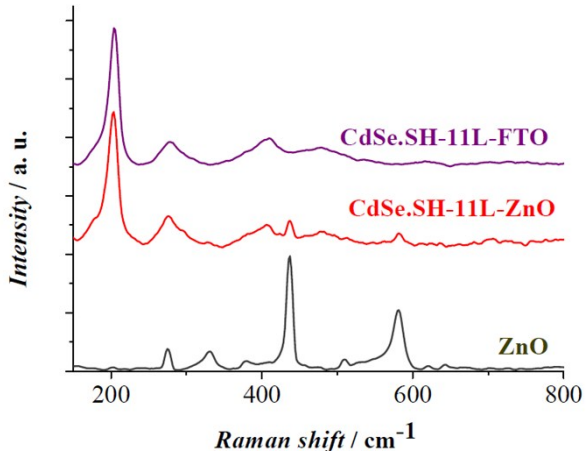

Figure S4. Experimental Raman spectra of a) 7, b)9 and c) 11 layers thick CdSe.SH NPLs, of ZnO nanorod arrays sensitized by the same NPLs and of bare ZnO nanorod arrays.

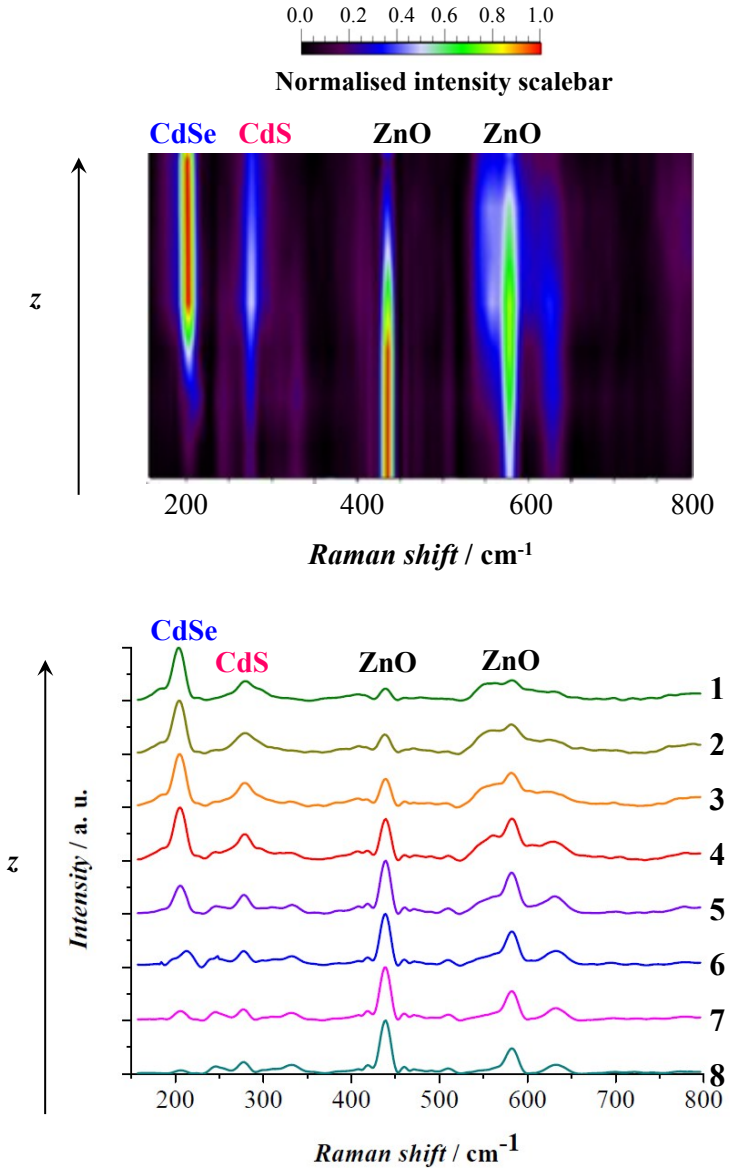

Figure S5. Two representations of the depth Raman profile of ZnO nanorod arrays sensitized by 7 layers thick CdSe.SH NPLs. The arrow indicating the z direction points towards the CdSe.SH nanoplatelet-coated surface of the sample.

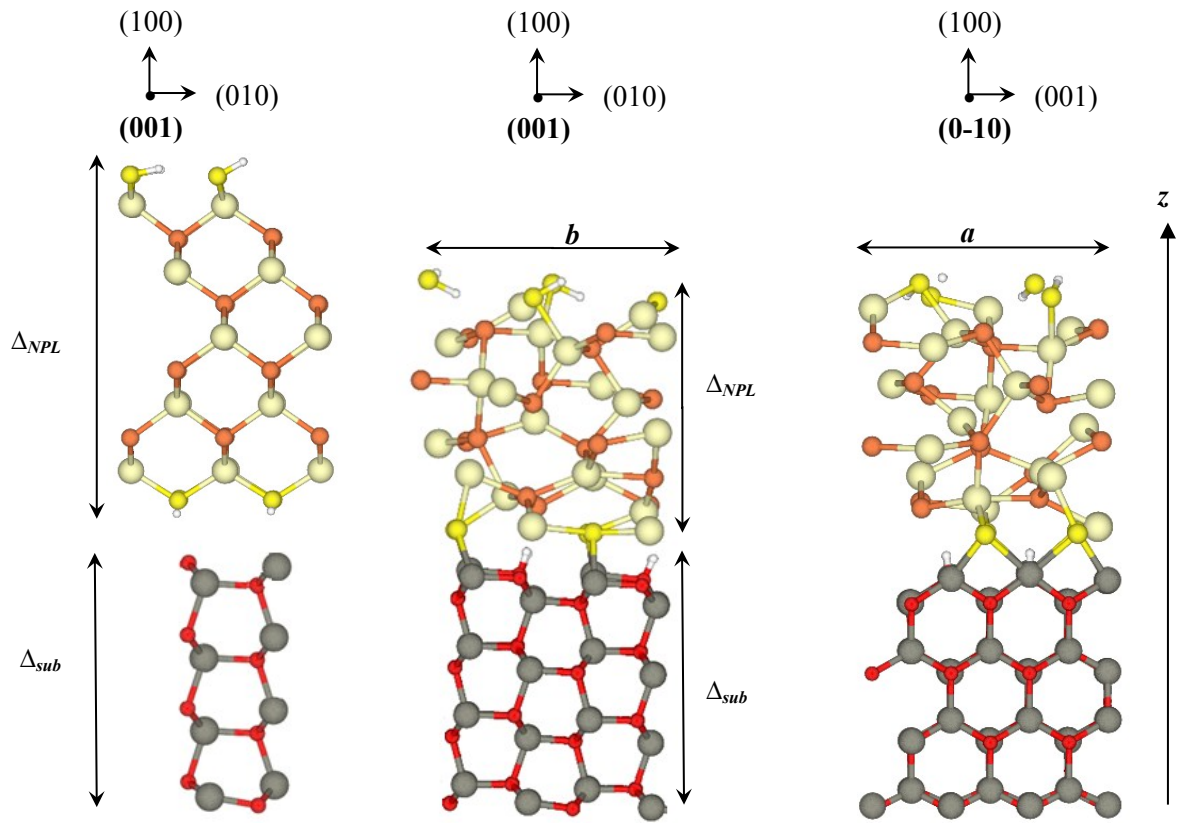

Figure S6. a) Structure of the isolated subsystems: 9 layers thick (5L) CdSe.SH and 8 layers thick (8L) ZnO slabs. b) Optimized geometry of the CdSe.SH (9L) – ZnO (8L) heterostructure, viewed along the (001) and (0-10) directions.

	CdSe.SH (9L) NPL	ZnO (8L) slab	Optimized CdSe.SH (9L)– ZnO (8L) interface
a	8.79	9.93	9.88
b	8.79	10.50	10.33
Δ_{NPL}	16.16	--	11.69
Δ_{sub}	--	9.42	9.89
γ	90.00	90.00	90.25
d (Cd-Se)	2.67-2.70	--	2.59-2.84
d (Cd-S)	2.60	--	2.52-2.68
d (Zn-S)	--	--	2.39-2.69
d (O-H)	--	--	0.98-1.00
d^1 (Zn-O)	--	1.86	2.05-2.08
d^2 (Zn-O)	--	2.00	2.00
δ_z (Zn)	--	--	0.78
δ_z (O)	--	--	0.33

Table S1. Lattice parameters (a, b in Å and γ in degrees) and interatomic distances of the isolated subsystems and the optimized CdSe.SH (9L) – ZnO (8L) heteostructure. d^1 and d^2 correspond to Zn-O distances in the uppermost ZnO slab layer and in the second layer, respectively. . δ_z^1 (Zn) and δ_z^1 (O) are the shifts, upon optimization, of Zn and O atoms along the z axis compared to their initial positions in the uppermost layer of the ZnO slab.

a)

b)

c)

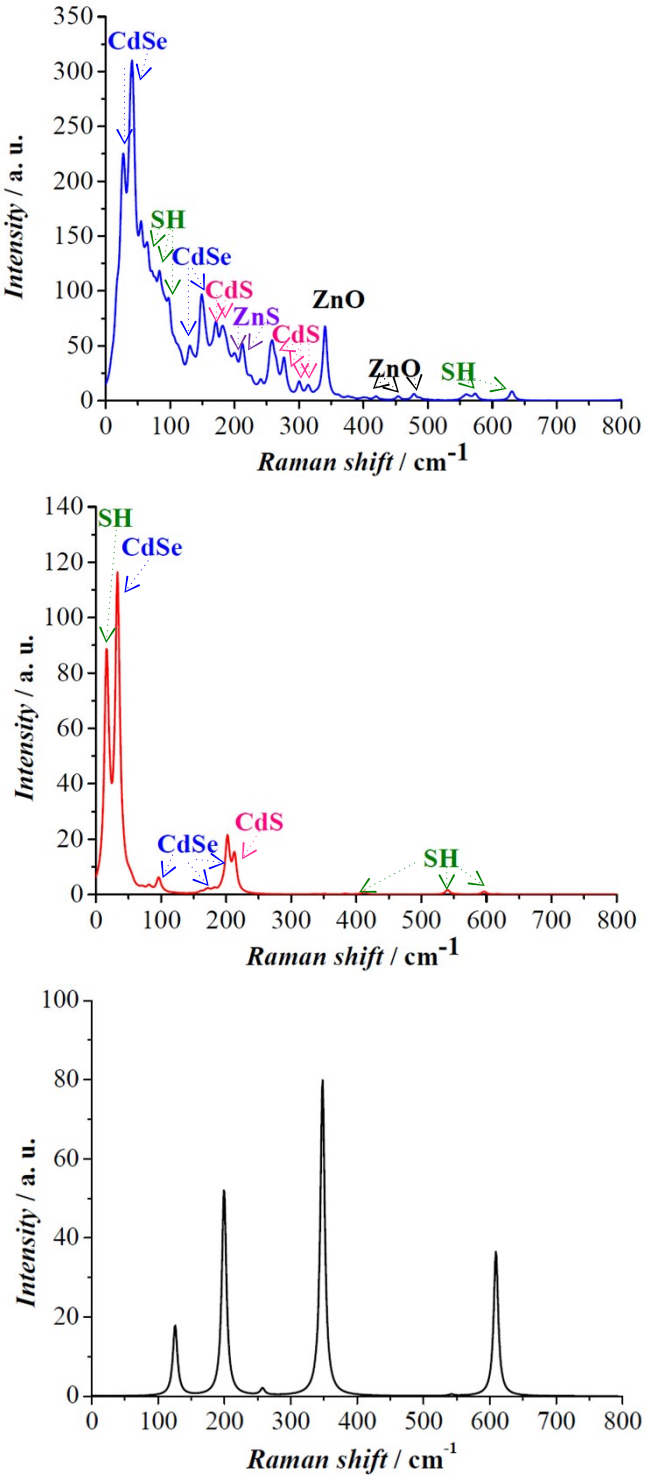

Figure S7. Computed Raman spectra of a) the CdSe.SH (9L) - ZnO system b) a 9 layers thick CdSe.SH slab and c) the uppermost layer of a ZnO wurtzite (10-10) slab.

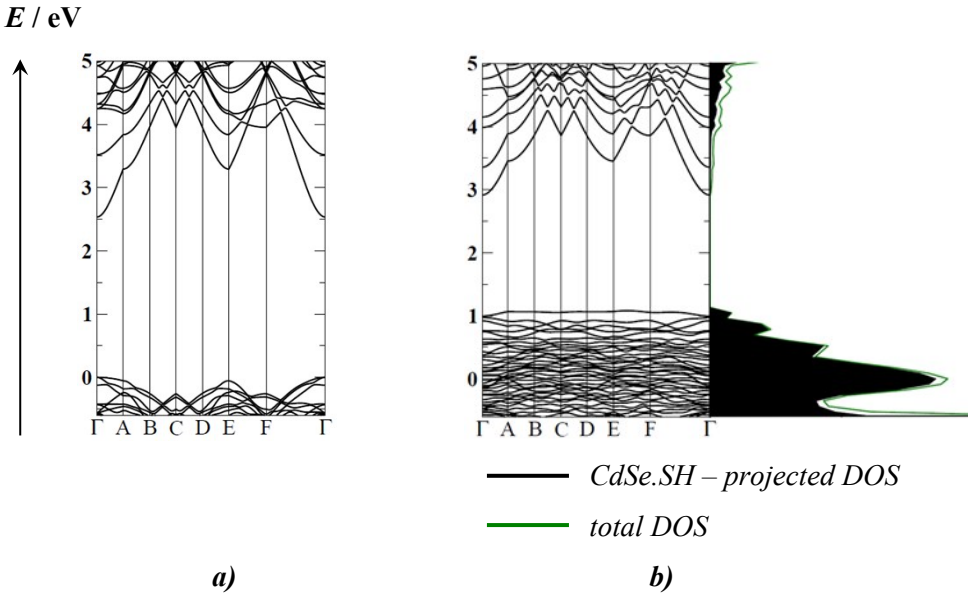

Figure S8. Band structures and density of states (DOS) of a) the bare 9 layers thick CdSe.SH slab and b) the CdSe.SH (9L) – ZnO (8L) heterostructure. The Fermi energy of the bare 9 layers thick CdSe.SH slab was chosen to be the zero of energy in each figure. The k points in the reciprocal space were defined as Γ (0 0 0), A $\left(0\,\frac{1}{3}\,0\right)$***, B*** $\left(\frac{1}{3}\frac{1}{3}\frac{1}{3}\right)$***, C*** $\left(\frac{2}{3}\frac{1}{3}\frac{2}{3}\right)$***, D*** $\left(\frac{2}{3}\frac{2}{3}\frac{2}{3}\right)$***, E*** $\left(\frac{3}{3}\frac{2}{3}0\right)$***, F*** $\left(\frac{2}{3}\frac{1}{3}0\right)$***.***

	CdSe.SH 5L	**ZnO 8L**	**CdSe.SH (5L) - ZnO**
Top of VB in *k*-space	Γ (0 0 0)	Γ (0 0 0)	W $\left(\frac{4}{6}\frac{3}{6}\frac{4}{6}\right)$
Bottom of CB in *k*-space	Γ (0 0 0)	Γ (0 0 0)	Γ (0 0 0)
	CdSe.SH 9L	**ZnO 8L**	**CdSe.SH (9L) - ZnO**
Top of VB in *k*-space	Γ (0 0 0)	Γ (0 0 0)	W $\left(\frac{4}{6}\frac{3}{6}\frac{4}{6}\right)$
Bottom of CB in *k*-space	Γ (0 0 0)	Γ (0 0 0)	Γ (0 0 0)

Table S2. Characteristics of the computed band gaps of the isolated subsystems and the constructed heterostructure

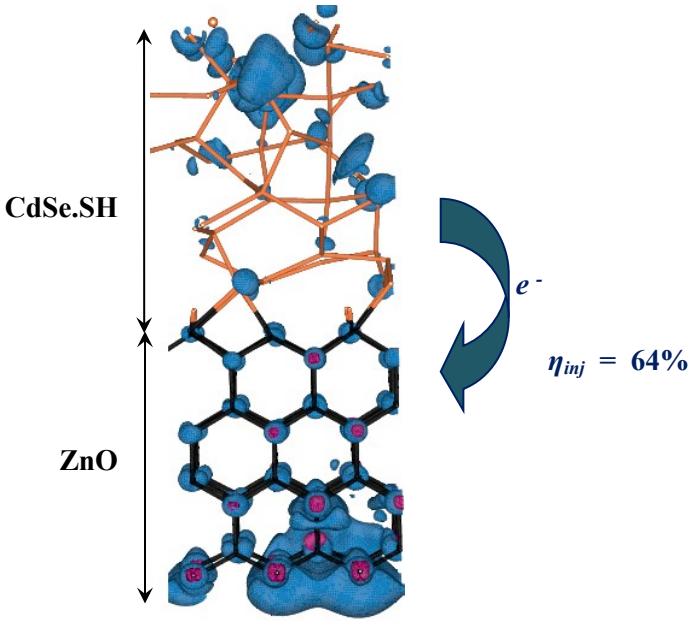

Figure S9. Spin density of the reduced CdSe.SH (5L)–ZnO system (excess of alpha electron is indicated in blue), isosurface contour value: 0.00034 a.u.